AIAA JOURNAL
Vol. 40, No. 3, March 2002

Turbulence Models in Pulsating Flows

Alberto Scotti*
University of North Carolina, Chapel Hill, North Carolina 27599
and
Ugo Piomelli†
University of Maryland, College Park, Maryland 20742

The performances of four low-Reynolds-number models are compared for the unsteady Reynolds-averaged Navier–Stokes equations applied to the flow in a channel driven by a pressure gradient oscillating around a nonzero mean. The models considered are the one-equation Spalart–Allmaras model, the k–ε model with the wall functions of Lam and Bremhorst, the k–ω^2 model of Saffman and Wilcox, and the k–ε–v^2 model of Durbin. The results are compared with experiments, direct simulations, and large-eddy simulations. The models give similar and reasonably accurate results as far as predicting the velocity profile in the channel as a function of the phase and reproduce the observed behavior during part of the cycle. However, large differences exist between the models themselves, as well as with respect to the large eddy simulations, at the level of the Reynolds shear stress, turbulent kinetic energy, and dissipation rate. The k–ε–v^2 model is overall superior to the other models considered.

Introduction

MANY turbulent flows, both natural (the gravity-wave-induced bottom boundary layer, the blood flow in large arteries, the flow around swimming fish, etc.) and artificial (flows in internal combustion engines, heat exchangers, and so on), are inherently unsteady. The unsteadiness can be caused by fluctuations in the driving force, to unsteadiness in the boundary conditions, or to a combination of both. The imposition of external unsteadiness can significantly alter a flow, even resulting in partial or full relaminarization of an initially turbulent flow. Despite their importance to a variety of fields and the complexity of the modifications that result from the unsteadiness, flows of this kind have received relatively little attention compared to steady ones. Although models for the unsteady Reynolds-averaged Navier–Stokes (URANS) equations are routinely used in engineering calculations, their accuracy, especially in view of the alterations of the turbulence physics that can take place in these flows, has not been carefully established.

In this paper we will compare the performance of four low-Reynolds-number URANS models applied to the flow in a channel driven by a pressure gradient oscillating around a nonzero mean. The simplicity of the geometry makes it possible to perform direct simulations and well-resolved large-eddy simulations that can be used to validate the URANS models. Furthermore, an analytical solution exists for laminar flow (a simple extension of Stokes' second problem[1]), and experimental data are available. Indeed, the present understanding of this kind of flows is based mainly on experiments carried out by four groups in the last 20 years: the Grenoble group,[2–4] the Iowa group,[5,6] the Illinois group,[7–9] and the Stanford group.[10,11]

The flow is controlled by three parameters. The mean pressure gradient ensures that the turbulent quantities oscillate around a nonzero mean. The mean wall stress can be used to define a mean friction velocity u_τ that, in conjunction with the viscosity ν, defines wall units. A second parameter is the forcing frequency $\Omega^+ = \Omega\nu/u_\tau^2$, or alternatively the Stokes length $l_s^+ \equiv (2/\Omega^+)^{1/2}$, a measure of how far the vorticity waves generated by the unsteady pressure gradient penetrate the laminar flow. The ratio between oscillating and steady centerline velocity a_{uc} completes the parameter space; when $a_{uc} < 1$ (current-dominated flow), experiments show that the flow is largely controlled by Ω^+; we will concentrate on this case, which is prevalent in the ocean,[12] and has been extensively investigated in the laboratory. Table 1 summarizes the parameters used in this study, as well as the ones used in the experiments discussed earlier.

The experimental evidence shows that at very low frequencies the turbulence has time to relax to the local (in time) equilibrium. As the frequency is increased, however, typical turbulent quantities such as the ratio between the intensity of streamwise fluctuation and the turbulent kinetic energy begin to exhibit a phase dependence, which might indicate that production and dissipation are out of phase. In this regime the flow can transition from a fully turbulent state to a quasi-laminar one within a wave cycle. At very high frequencies the flow can be assumed to be the superposition of a steady part plus the laminar Stokes solution for the given frequency. In this regime the unsteadiness is confined within the viscous sublayer, while the turbulence in the outer layer is frozen and oscillates as a plug flow. The effects of the steady flow on the oscillating part are more subtle. The most notable (and counterintuitive) one is the fact that, for $0.02 < \Omega^+ < 0.06$, the amplitude of the oscillation of the wall stress is lower than the value it would have were the flow to be purely laminar. In other words, the background turbulence can reduce the shear.

Despite its simplicity, this flow is an extremely challenging test case for URANS models. The fact that turbulence is out of equilibrium and that the relaminarization and retransition can take paths dependent on the frequency constitutes a severe challenge for conventional URANS models. However, most of the models used in the literature are extensions of steady eddy-viscosity closures, with different recipes to compute the eddy viscosity,[13–14] with the exception of a model proposed by Mankbadi and Liu,[15] which is based on rapid distortion theory and one introduced by Mao and Hanratty[7] to explain the reduction in shear observed at intermediate frequencies. Thus, a better understanding of the capabilities and limitations of URANS models is required. Direct and large-eddy simulation data can be very useful in helping to achieve this goal, similarly to the fundamental role they have played in expanding the understanding of canonical boundary layers.[16–18] It is somewhat surprising then to observe that only a handful of studies have been conducted on the subject at hand. Spalart and Baldwin[19] performed direct numerical simulation (DNS) of a purely oscillating flow in the transitional regime, whereas more recently Hsu et al.[20] used large eddy simulation (LES) to validate a RANS model, again in the purely oscillating case. Scotti and Piomelli[21] used LES and DNS to investigate

Received 30 April 2001; revision received 9 May 2001; accepted for publication 9 June 2001.

*Assistant Professor, Department of Marine Sciences.
†Professor of Mechanical Engineering, Department of Mechanical Engineering. Senior Member AIAA.

Table 1 Parameters used in the the experiments cited

Group	Geometry	Ω^+	Re	a_{uc}
Grenoble[2–4]	Channel	0.001–0.25	5.0×10^3–10×10^3	0.14–0.64
Iowa[5,6]	Pipe	0.00079–0.0057	25×10^3	0.15–0.64
Illinois[7–9]	Pipe	0.21–0.0075	7.5×10^3–35×10^3	0.044–0.3
Stanford[10,11]	Flat plate	0.0165–0.00077	27×10^3	0.15
Present study	Channel	0.02–0.0008	7.2×10^3	0.7

oscillating channel flows and confirmed the reduction in shear stress at the wall for intermediate driving conditions. In this paper we will use the databases generated by Scotti and Piomelli[21] to test four well-established URANS models. We limit ourselves to the study of eddy-viscosity models, which are in more widespread use, especially among users of commercial software. In the following, after briefly reviewing the numerical dataset used as benchmark we will describe the models used. Then, the models will be evaluated a priori (using the data from the LES and DNS to compute the Reynolds stresses according to the prescription of the model) and a posteriori (comparing the URANS results with LES and DNS). At the end some conclusions will be drawn.

Problem Formulation and Numerical Data Sets

We have simulated the flow in a channel with periodic boundary conditions in the spanwise and streamwise directions. The geometry is sketched in Fig. 1. The flow is forced by a pressure gradient given by

$$P_f(x,t) = \Delta P_0[1 + \alpha \cos(\Omega t + \pi/2)]x/L_x \tag{1}$$

so that the flow begins the acceleration phase at $\Omega t \equiv 2\pi t/T = 0$. By setting $\Delta P_0/L_x = 1.0 \times 10^{-4}$, the Reynolds number based on the mean friction velocity $u_\tau = \sqrt{(H\,\Delta P_0/2\rho L_x)}$ and channel half-height is equal to 350, whereas the one based on the mean centerline velocity is approximatively equal to 7.2×10^3. In all calculations α was set to keep a_{uc} close to 0.7. The frequency Ω^+ was varied from 0.02 to 0.0008 (Table 1).

The reference data were obtained from DNS and LES of this flow, which were performed using a well-established spectral code.[22] The DNS used $128 \times 129 \times 192$ points in the streamwise, wall-normal, and spanwise directions to discretize a domain whose size was $3\pi H \times H \times \pi H$ (H is the channel height). The LES used $64 \times 65 \times 64$ points to discretize the same domain, and the subgrid-scale stresses were modeled using the dynamic eddy-viscosity model.[23,24] The LES were validated by comparison with the DNS at high frequency and with experiments at intermediate and low frequencies and found to be in good agreement with the existing data.[21] Detailed comparisons between the LES, DNS, and experiments, a more complete description of the flow physics and a discussion of the numerical code, are beyond the scope of the present paper. The interested reader is referred to Scotti and Piomelli[21] for the physical aspects and Piomelli et al.[25] for the numerics.

Description of the URANS Models

Because of the simple geometry, the URANS equation for the horizontal momentum simply becomes

$$\frac{\partial U}{\partial t} = -\frac{\partial P_f}{\partial x} + \frac{\partial}{\partial y}\left(\nu \frac{\partial U}{\partial y} - \langle u'v' \rangle\right) \tag{2}$$

where $\langle \cdot \rangle$ denotes phase averaging, defined as

$$\langle f \rangle \left(y, \frac{t}{T}\right) = \frac{1}{N} \sum_{n=1}^{N} \frac{1}{L_x L_z} \int_0^{L_x} \int_0^{L_z} f\left(x, y, z, \frac{t}{T} + n\right) \mathrm{d}z\, \mathrm{d}x \tag{3}$$

and $U = \langle u \rangle$. We have selected four commonly used URANS model for this study. In order of increasing computational complexity, they are the one-equation model of Spalart and Allmaras,[26] a standard k–ε model with the wall correction of Lam and Bremhorst,[27,28] the k–ω^2 model of Saffman and Wilcox,[29,30] and the k–ε–v^2 model of Durbin.[31] All models assume the existence of an eddy viscosity that is used to express the Reynolds stress as

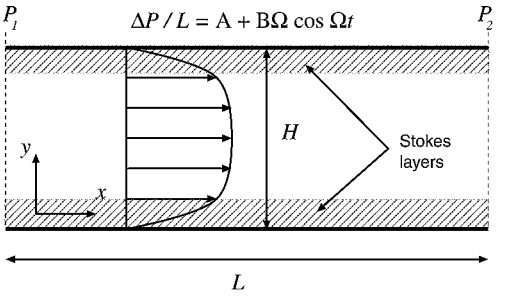

Fig. 1 Sketch of the channel geometry.

$$-\langle u'v' \rangle = \nu_t \frac{\partial U}{\partial y} \tag{4}$$

Next, we briefly review each model, and we indicate the parameters used. All of the models were run first with a steady pressure gradient, and the results compared with the DNS data of Moser et al.[32] for channel flow at $Re_\tau = 395$. (The DNS data were also used to provide the initial condition.) These runs were used to calibrate the constants in the models. In practice, only the k–ε–v^2 model required some deviation from the published values.

Spalart–Allmaras One-Equation Model

The Spalart–Allmaras[26] one-equation model (in the following referred to as SA) is gaining increased popularity for the calculation of aerodynamic flows, both in the context of steady or unsteady RANS calculations and in the approach known as detached eddy simulation.[33] In this model a nonlinear transport equation is solved for the eddy viscosity. This equation includes the effects of production, diffusion, wall blocking, destruction and finite Reynolds number near the wall. All terms in the equation are developed based on phenomenological considerations.

k–ε Two-Equation Model

The k–ε model might be the most commonly used model in engineering applications. The eddy viscosity is given by

$$\nu_t = C_\mu (k^2/\varepsilon) \tag{5}$$

where k is the phase-averaged turbulent kinetic energy and ε the phase-averaged rate of dissipation. Transport equations for the turbulent kinetic energy k and the dissipation ε are then solved. Many formulations of this model exist, and especially the near-wall treatments can differ significantly. Our choice of the model proposed by Lam and Bremhorst[27] was motivated by the fact that this formulation does not require the use of the instantaneous u_τ. In the configuration under study, the flow can reverse its direction, and the phase-averaged wall stress might vanish. This feature makes any model that requires the use of wall variables liable to fail. We refer to this model as KE.

k–ω^2 Model

The k–ω^2 model (KO2 in the following) was initially proposed by Saffman[29] and later modified by Saffman and Wilcox.[30] The eddy viscosity is assumed to be

$$\nu_t = k/\omega \tag{6}$$

Table 2 Original and modified parameters in the k–ε–v^2 model

Parameter	C_μ	C_{ε_2}	C_1	C_2	C_L	C_η
Original	0.19	1.9	1.4	0.3	0.3	70
Modified	0.21	1.9	1.22	0.4	0.2	80

where ω is the phase-averaged pseudo vorticity, for which a transport equation (written for ω^2) is given, including the effects of production, diffusion, and dissipation. This model does not make use of low-Reynolds-number corrections, unlike the more studied k–ω formulation of Wilcox.[34] This model has been used in several studies to model the boundary layer induced by surface gravity waves[35–37] without a nonzero mean current. To the best of our knowledge, it has never been tested in the presence of a mean current.

k–ε–v^2 Model

The k–ε–v^2 (referred to as KEV2) model proposed by Durbin[31] represents an extension of the standard k–ε model. The eddy viscosity is taken to be

$$\nu_t = C_\mu(\langle v^2\rangle k/\varepsilon) \tag{7}$$

where $\langle v^2\rangle^{1/2}$ is a velocity scale (in this geometry $\langle v^2\rangle$ represents the intensity of vertical fluctuations). To include the effects of the pressure-strain term (which is absent in the equation for k), an auxiliary equation is introduced that accounts for the blocking effect of the wall. We have calibrated the model using the DNS data at $Re_\tau = 395$ (Ref. 32), resulting in slightly different values for some of the coefficients, compared to their standard ones. The values used are shown in Table 2.

Numerical Aspects

The URANS equation (2) was solved using the same numerical scheme for all models. The spatial discretization was performed using second-order finite differences on a nonuniform grid (stretched to accommodate 10 points within $y^+ < 10$). The derivatives of $\langle v^2\rangle$ in the KEV2 model, however, were computed using a fourth-order scheme because $\langle v^2\rangle \sim y^{+4}$ near the wall, so that a second-order scheme would produce errors of the the same order as the derivative itself. A third-order Runge–Kutta scheme was used to advance the nonlinear part of the equations, while the linear part was treated implicitly with a Crank–Nicholson scheme. The initial conditions were obtained from the LES data. The model was run for a total of 10 wave cycles to remove initial transients.

Physical Description of the Flow

Details of the flow can be found elsewhere.[21] For the sake of completeness, however, we summarize briefly the main physical properties.

The unsteady pressure gradient at the wall generates waves of vorticity that propagate away from the wall, while being attenuated. Assuming that the effect of turbulence can be captured, at least qualitatively, by a simple eddy viscosity ν_t, and drawing an analogy to the laminar Stokes problem, the effect of the oscillation on the flow should be confined to a layer of thickness of order l_t, where

$$l_t = [2(\nu + \nu_t)/\omega]^{\frac{1}{2}} \tag{8}$$

is a turbulent Stokes length obtained using the sum of the molecular and turbulent diffusivities. Taking for the eddy viscosity $\nu_t = \kappa u_\tau l_t$, where κ is the von Kármán constant, it follows that

$$l_t^+ = l_s^+\left[\left(\kappa l_s^+/2\right) + \sqrt{1 + \left(\kappa l_s^+/2\right)^2}\right] \tag{9}$$

Thus, in turbulent flow the penetration length, l_t^+ is proportional to l_s^+ at high frequencies; at low frequencies, however, l_t^+ scales as l_s^{+2}. Only if l_t^+ is large enough inner and outer layer are significantly coupled; in our calculations that was the case at intermediate and low frequencies. At high frequencies, on the other hand, the turbulence in the outer zone is convected by the oscillating flow as a plug flow.

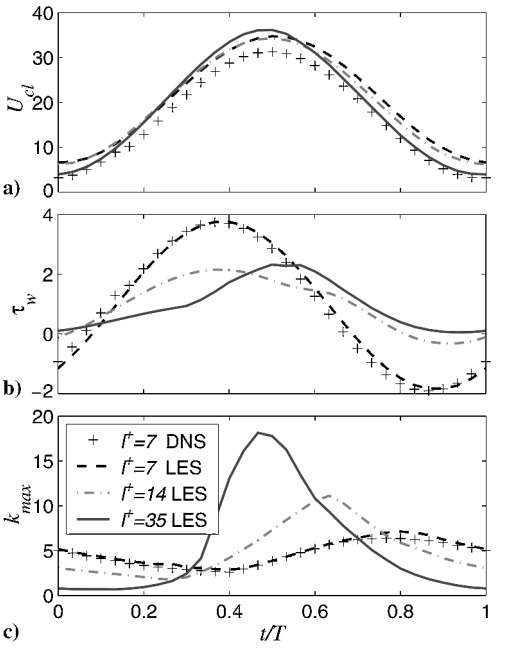

Fig. 2 Time series of the phase-averaged a) centerline velocity, b) wall stress, and c) maximum of the turbulent kinetic energy k. A phase lag of $\pi/4$ corresponds to $t/T = 0.125$.

The centerline velocity, shown in Fig. 2, lags behind the stress at the wall; the phase difference is $\pi/4$ at high frequencies and drops to zero at low frequencies, where the flow is essentially in equilibrium (unless otherwise stated, all quantities are normalized using the time-averaged friction velocity u_τ). The good agreement between DNS and LES at the high frequency can also be observed in this figure. At high frequencies the response of the system is essentially at the driving frequency, despite the nonlinear character of the equations. As the frequency is lowered, however, higher harmonics are excited.

It is interesting to note the asymmetric response of the turbulent kinetic energy at low and intermediate frequencies: at the lowest frequencies the flow at the beginning of the acceleration phase is essentially laminar (although the velocity profile is not, as the viscous time needed to relax to the Poiseuille profile $t^+ \sim Re_\tau^2$ exceeds the period). As the flow picks up momentum, very long and smooth streaks develop, which, eventually, become unstable and burst into a localized turbulent spot, at $t = 3T/8$, which eventually fills the whole channel. At high frequencies the process is very different. Fairly healthy streaky structures can be observed for the entire period. During the acceleration phase, the flow begins to relaminarize: some very long, nearly straight low-speed streaks can be observed ($\frac{1}{8} \le t/T \le \frac{2}{8}$; see Figs. 21 and 22 in Ref. 21).

A Priori Testing

A first evaluation of the model accuracy can be performed a priori by computing the Reynolds stresses and the eddy viscosity using the "true" velocity field, represented here by the LES data. This is possible only for KE and KEV2 because SA and KO2 use quantities that do not have a direct physical counterpart. This comparison allows us to evaluate the validity of the modeling ansatz in itself, removing possible errors that can be caused by the modeling of the terms in the k or ε equations. Accordingly, we have computed the Reynolds stresses from Eq. (4) using the LES data for U, k, ε, and $\langle v^2\rangle$ in Eqs. (5–7).

The peak Reynolds shear stress is shown in Fig. 3 for the KE and KEV2 models. KEV2 is able to reproduce the maximum value of the phase-averaged Reynolds shear stress fairly well, although at low frequencies it tends to overestimate the stress growth during the acceleration phase. The performance of KE is poorer: the peak Reynolds shear stress is very significanly overestimated during the acceleration phase.

Significant differences between the two models can be observed in the shapes of the profiles as well, which are shown in Fig. 4,

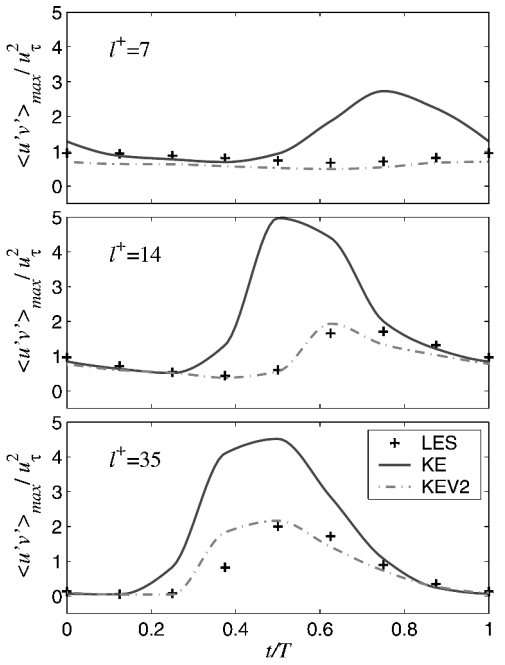

Fig. 3 Time series of the maximum phase-averaged Reynolds shear stress $\langle u'v' \rangle$.

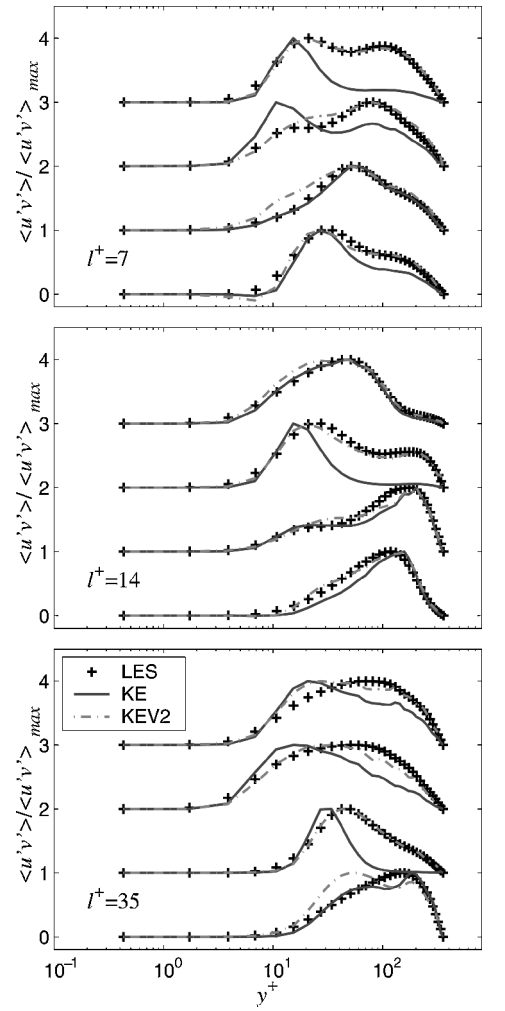

Fig. 4 A priori evaluation of the Reynolds stress $\langle u'v' \rangle$ using LES data. Profiles are plotted every $T/4$ and offset in the vertical direction; the bottom plot corresponds to $t/T = 0$.

normalized by their maximum value. KEV2 is able to reproduce the shape of the Reynolds stress fairly well, the most notable exception being a tendency during the acceleration phase to overestimate the stress growth in the inner region. With the KE model, on the other hand, not only is the peak stress in the inner region much larger than observed in the LES, but also the relative stress in the outer region is often too small. Although the former fact could be ameliorated by a different choice of wall functions, the latter result should be viewed as an intrinsic shortcoming of the of the k^2/ε ratio. The acceleration phase, in fact, is accompanied by a decrease in the structure parameter

$$a_1 = -\langle u'v' \rangle / 2k \tag{10}$$

which indicates that turbulence is less efficient in extracting shear from the available energy.[21] This decrease is characteristic of the response of many turbulent flows when they are perturbed from equilibrium. In this flow it is also accompanied by a decrease in the dissipation ε during the relaminarization that takes place during the acceleration; thus, the eddy viscosity predicted by the KE model increases (the denominator decreases, while the numerator decreases less rapidly than the shear stress), while the actual Reynolds stress decreases.

A Posteriori Testing

We now compare a posteriori the predictions of the URANS models with the LES data. Figure 5 shows the phase-averaged streamwise velocity profiles at intervals of $T/4$. All of the model predictions are in reasonable agreement with the LES data. The agreement

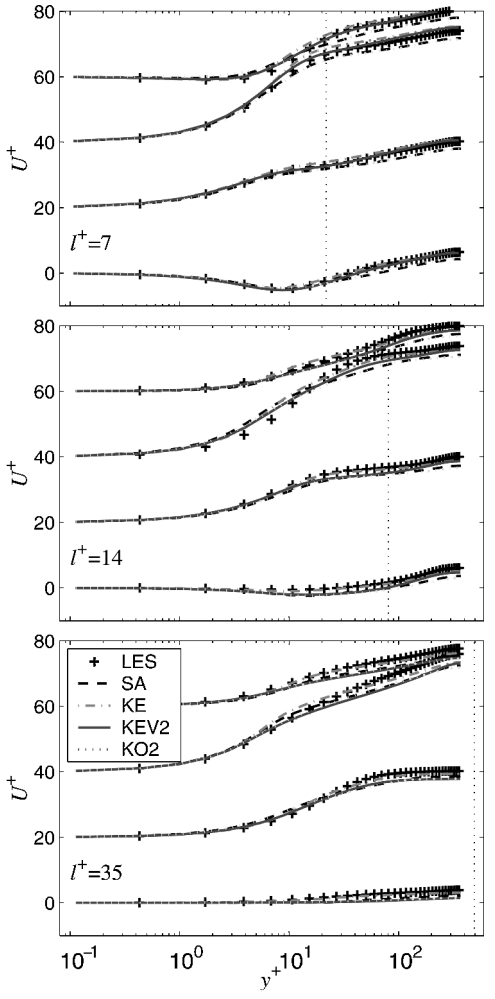

Fig. 5 Profiles of the phase-averaged streamwise velocity. Profiles are plotted every $T/4$ and offset in the vertical direction; the bottom plot corresponds to $t/T = 0$. The dotted line corresponds to the turbulent penetration length l_t^+ given by Eq. (9).

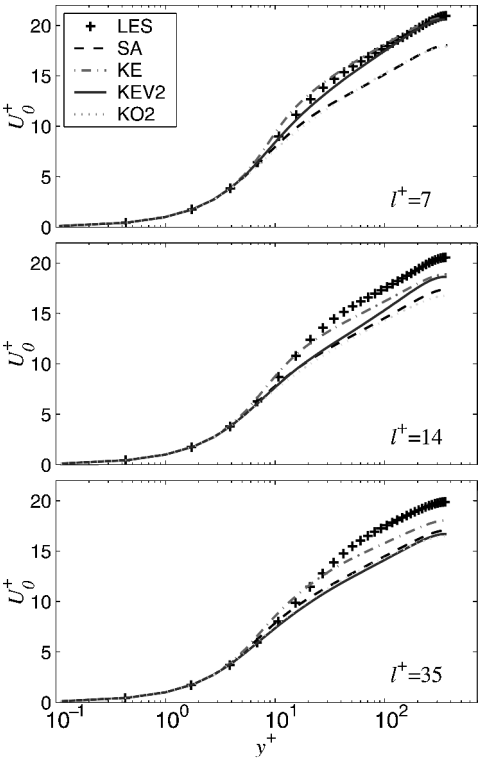

Fig. 6 Time-averaged streamwise velocity.

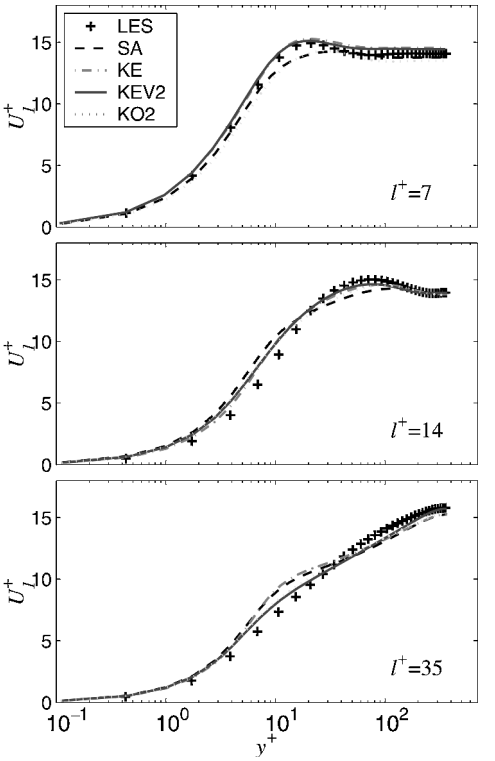

Fig. 7 Streamwise velocity component at the forcing frequency.

between models and LES is generally better for $y^+ > l_t^+$, i.e., outside the layer affected by the unsteadiness [recall that the turbulent penetration length was defined in Eqs. (8) and (9)]. At high frequency KE and KEV2 are very close to each other and essentially match the LES. SA departs from the LES profile more consistently, especially at the end of the deceleration phase (top profile). KO2 can be hardly distinguished from SA. At intermediate frequencies the discrepancy between URANS models and LES is more evident, especially during the deceleration phase.

A significant contribution to the differences between the models and the LES is caused by the error in the prediction of the time-averaged velocity:

$$U_0^+ = \frac{1}{T}\int_0^T \langle U^+ \rangle \, \mathrm{d}t \tag{11}$$

which is shown in Fig. 6. All models underpredict the ratio U_b/u_τ (where U_b is the average velocity in the channel) by as much as 20% in some cases. The KE model is perhaps the most accurate throughout the range of frequencies, a surprising finding given the results obtained from the a priori tests just described.

To evaluate the response of the models to the unsteadiness, we can consider the component of the phase-averaged velocity at the driving frequency, which is obtained by minimizing in the least-squares sense the function

$$\mathrm{err}(z,t) = U(z,t) - U_0(z) - U_1(z)\cos[\Omega t + \alpha(z)] \tag{12}$$

where Ω is the driving frequency. U_1^+ is shown in Fig. 7. The KEV2 model appears to be the most accurate in reproducing the response of the flow to the unsteadiness, at least as far as the streamwise velocity is concerned.

In our calculations the mean value of the wall stress is determined by the mean pressure gradient, whereas its oscillating part depends on the amplitude and frequency of the pressure-gradient oscillations. At large driving frequencies the amplitude tends to the one predicted by laminar theory. At low frequencies the ratio of the turbulent to laminar stress diverges as $\omega^{-1/2}$ (see Tardu et al.[2]). The two regimes are separated by range of frequencies in which the amplitude is lower than the laminar value, a result that has been observed in several experiment,[2,7,38] and confirmed by the LES (Fig. 8). At high

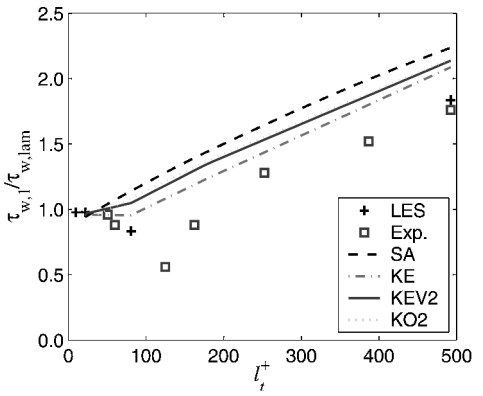

Fig. 8 Amplitude of the component of the wall stress at the driving frequency, normalized with the amplitude of the wall stress in a laminar flow driven at the same frequency.

frequencies all of the models predict a slightly higher value of the amplitude. As the frequency is lowered, the models fail to reproduce the reduction in amplitude observed experimentally and by the LES.

We consider next the Reynolds shear stress, shown in Fig. 9. At high frequency the models predict the correct behavior during the acceleration phase, especially outside the region $y^+ = 2l_t^+$. In the region affected by the vorticity waves, on the other hand, the Reynolds-stress increase that is observed in the LES at the beginning of the deceleration phase is overestimated by all models. Also, the increase begins too early. This is also clearly shown in Fig. 10, in which the peak $\langle u'v' \rangle$ is shown. The substantial overestimation of $\langle u'v' \rangle_{\max}$ by the KE model that was observed in the a priori tests is not present here, indicating that the self-correcting features of the model improve the results. Of the four models tested, KEV2 appears to be the most accurate.

At intermediate frequencies we observe similar trends. The SA and KO2 model severely overestimate the stress increase coinciding with the onset of deceleration. KE and KEV2 fare better during acceleration, but behave in a manner similar to SA during the deceleration, although with a smaller error. The early beginning of the Reynolds-stress increase is at this frequency most notable (Fig. 10).

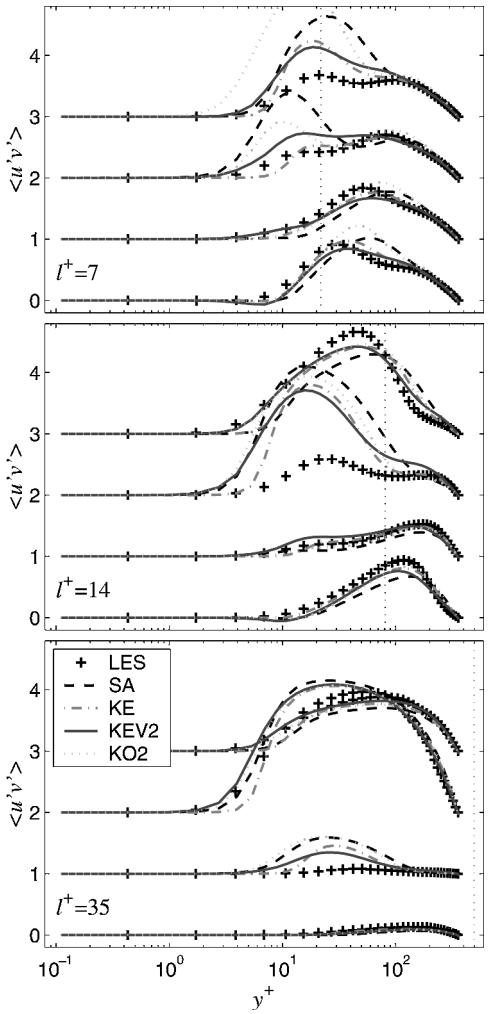

Fig. 9 Profiles of the phase-averaged Reynolds shear stress. Profiles are plotted every $T/4$ and offset in the vertical direction; the bottom plot corresponds to $t/T = 0$; · · · ·, turbulent penetration length l_t^+ given by Eq. (9).

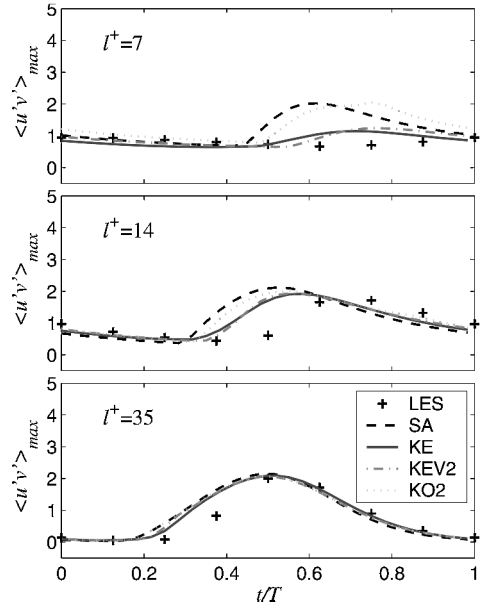

Fig. 10 Time series of the maximum phase-averaged Reynolds shear stress $\langle u'v' \rangle$.

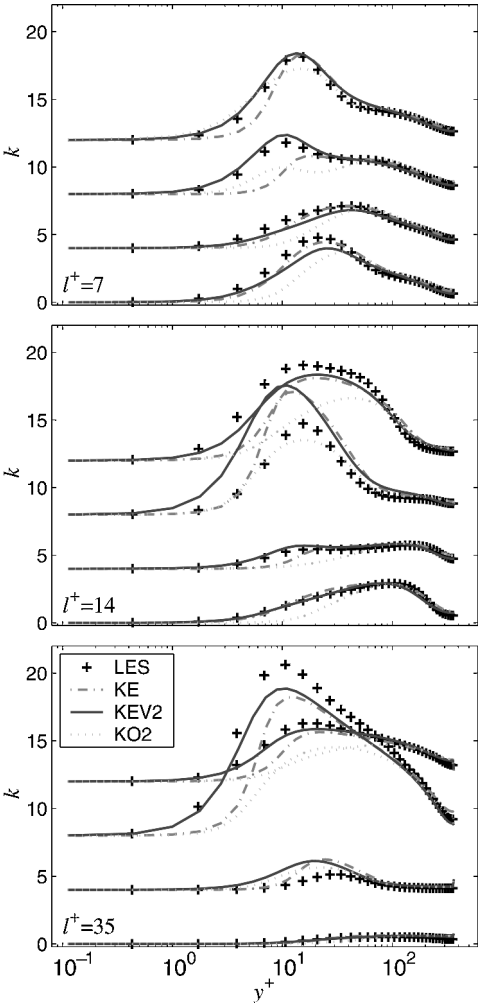

Fig. 11 Profiles of the phase-averaged turbulent kinetic energy k. Profiles are plotted every $T/4$ and offset in the vertical direction; the bottom plot corresponds to $t/T = 0$.

At low frequency similar conclusions can be drawn: the largest deviation occurs during the last stage of the acceleration phase. As shown before, the flow is essentially laminar during the early accelerating phase, and all of the models transition to turbulence early. URANS models of this type may have difficulties predicting transition. The SA model, in particular, assumes that the transition point is known and may not be expected to predict transition accurately.

In the case of KE, KO2, and KEV2, in addition to $\langle u'v' \rangle$ we can compare the phase-averaged turbulent kinetic energy k and rate of dissipation ε (the latter being equal to $0.09k\omega$ for KO2) modeled by the URANS with the one calculated from the LES. In Fig. 11 we show k. At high frequency KEV2 is in good agreement with the LES for the entire cycle, whereas KE agrees only during the accelerating phase; during the deceleration phase, the KE underestimates the turbulent kinetic energy in the region $y^+ < 2l_t^+$. In the same region KO2 is consistently lower than the LES, faring slightly better during the deceleration stage. At the intermediate frequency the situation is similar, but the difference between KEV2 and LES is larger, and at $t/T = \frac{1}{2}$ the peak energy predicted by KE is larger than in the LES, while KO2 gives a reasonably good agreement. Again, the acceleration phase and the late deceleration one are reproduced satisfactorily by KE and KEV, but not KO2. At the low frequency we observe a similar pattern, although during the deceleration phase the KE and KEV2 models have less (and KO2 much less) energy than the LES. Even in the steady case the energy predicted by the KE and KO2 models is lower in the inner layer than the LES and DNS.

Finally we show the dissipation ε in Fig. 12. KEV2 tends to have more realistic trends in the inner layer, but none of the models is particularly accurate. In the decoupled part of the outer layer, on the other hand, the agreement is good at all times.

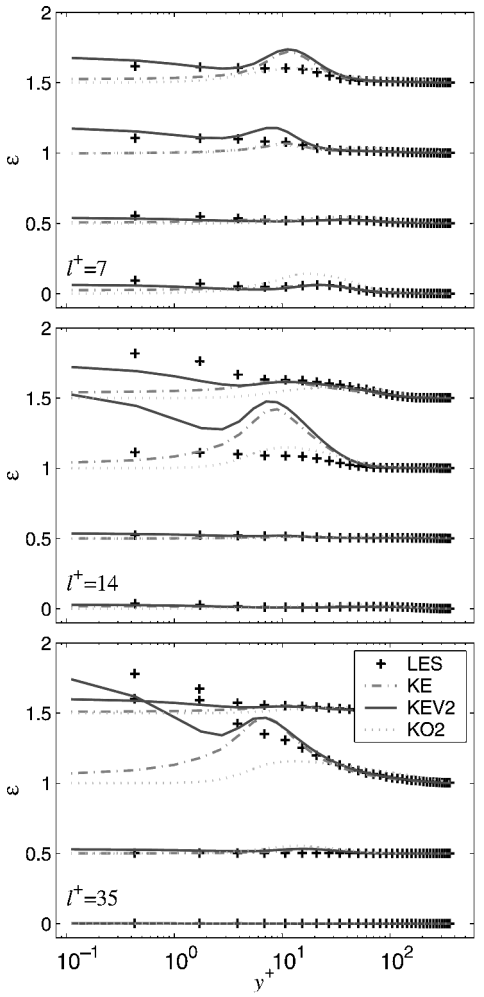

Fig. 12 Profiles of the phase-averaged turbulent kinetic energy dissipation ε. Profiles are plotted every $T/4$ and offset in the vertical direction; the bottom plot corresponds to $t/T = 0$.

Conclusions

In this paper we have considered four existing RANS models applied to a channel flow driven by an unsteady pressure gradient, using a combination of DNS and LES data as reference. The models in the portfolio were chosen to be "standard" representative within their category and have been used in the past to study this kind of flows; our intent was to provide a base for a qualitative and possibly quantitative assessment of their relative strenghts and weaknesses. Several interesting features have been brought to attention. A priori testing shows that the KEV2 model has the potential for giving a fairly accurate estimate of the Reynolds stress, provided that the coefficient C_μ is adjusted. On the other hand, it seems difficult to come up with a satisfactory solution to cure the pitfalls of KE, which appear to be structurally related to setting $\nu_t \sim k^2/\varepsilon$.

The a posteriori tests show a more benign outcome. Despite large differences in the Reynolds shear stress relative to the LES, the time evolution of the streamwise velocity seems relatively unaffected. The picture is actually quite complex because we have to consider simultaneously both the effects on the mean (time-averaged) flow and on its oscillating part. Indeed, changes in the oscillating eddy viscosity will affect the mean flow via a rectification mechanism; vice versa, changes in the mean eddy viscosity will show up in the oscillating velocity component.

We observe the centerline velocity predicted by the URANS models progressively decreasing as the frequency is lowered. Also, the largest deviation of the oscillating components of the flow occur during the deceleration phase, in which the predicted Reynolds shear stress is farther apart from the observed one. The discrepancies between the URANS models and the LES seem to be limited to about $\frac{1}{3}$ to $\frac{1}{4}$ of the period T. Thus, at high frequencies the errors are short-lived (compared to the diffusive timescale in the channel flow), whereas at lower frequencies the errors live longer and can redistribute momentum on a larger area.

As far as the streamwise velocity is concerned, all models considered perform just similarly, and their accuracy may be acceptable. If, on the other hand, information concerning the Reynolds stress is required, as is the case for instance in sediment transport or medical applications, the SA and KO2 models do not appear to give sufficient accuracy. Between KE and KEV2 overall the latter appears more accurate, although at the extra cost of solving two additional equations, compared with KE.

Acknowledgments

This work was supported by National Science Foundation under Grant OCE-99-10883 and by the Woods Hole Oceanographic Institute under Cooperative Agreement A100140.

References

[1]Stokes, G. G., "On the Effect of the Internal Friction of Fluids on the Motion of Pendulums," *Transactions of the Cambridge Philosophical Society*, Vol. 9, 1850, p. 8; reprinted in Stokes, G. G., *Mathematical and Physical Papers*, Cambridge Univ. Press, Cambridge, England, U.K., 1901.

[2]Tardu, S., Binder, G., and Blackwelder, R. F., "Turbulent Channel Flow with Large-Amplitude Velocity Oscillations," *Journal of Fluid Mechanics*, Vol. 267, 1994, pp. 109–151.

[3]Binder, G., Tardu, S., and Vezin, P., "Cyclic Modulation of Reynolds Stresses and Length Scales in Pulsed Turbulent Channel Flow," *Proceedings of the Royal Society of London, Series A*, Vol. 451, No. 1941, 1995, pp. 121–139.

[4]Tardu, S., and Binder, G., "Wall Shear Stress Modulation in Unsteady Turbulent Channel Flow with High Imposed Frequencies," *Physics of Fluids A*, Vol. 5, No. 8, 1993, pp. 2028–2037.

[5]Tu, S. W., and Ramaprian, B. R., "Fully Developed Periodic Turbulent Pipe Flow. Part 1. Main Experimental Results and Comparison with Predictions," *Journal of Fluid Mechanics*, Vol. 137, 1983, pp. 31–58.

[6]Ramaprian, B. R., and Tu, S. W., "Fully Developed Periodic Turbulent Pipe Flow. Part 1. The Detailed Structure of the Flow," *Journal of Fluid Mechanics*, Vol. 137, 1983, pp. 59–81.

[7]Mao, Z.-X., and Hanratty, T. J., "Studies of the Wall Shear Stress in a Turbulent Pulsating Pipe Flow," *Journal of Fluid Mechanics*, Vol. 170, 1986, pp. 545–564.

[8]Finnicum, D. S., and Hanratty, T. J., "Influence of Imposed Flow Oscillations on Turbulence," *Physico-Chemical Hydrodynamics*, Vol. 10, No. 5–6, 1988, pp. 585–598.

[9]Mao, Z., and Hanratty, T. J., "Influence of Large-Amplitude Oscillations on Turbulent Drag," *AICHE Journal*, Vol. 40, No. 10, 1994, pp. 1601–1610.

[10]Brereton, G. J., Reynolds, W. C., and Jayaraman, R., "Response of a Turbulent Boundary Layer to Sinusoidal Free-Stream Unsteadiness," *Journal of Fluid Mechanics*, Vol. 221, 1990, pp. 131–159.

[11]Brereton, G. J., and Reynolds, W. C., "Dynamic Response of Boundary-Layer Turbulence to Oscillatory Shear," *Physics of Fluids A*, Vol. 3, No. 3, 1991, pp. 178–187.

[12]Grant, W. D., and Madsen, O. S., "The Continental-Shelf Bottom Boundary Layer," *Annual Review of Fluid Mechanics*, Vol. 18, 1986, pp. 265–305.

[13]Gündoğdu, M. Y., and Çarpinlioğlu, M. Ö., "Present State of Art on Pulsatile Flow Theory (Part 1: Laminar and Transitional Flow Regimes)," *Japanese Society of Mechanical Engineering International Journal, Series B*, Vol. 42, No. 3, 1999, pp. 384–397.

[14]Gündoğdu, M. Y., and Çarpinlioğlu, M. Ö., "Present State of Art on Pulsatile Flow Theory (Part 2: Turbulent Flow Regime)," *Japanese Society of Mechanical Engineering International Journal, Series B*, Vol. 42, No. 3, 1999, pp. 398–410.

[15]Mankbadi, R. R., and Liu, J. T. C., "Near-Wall Response in Turbulent Shear Flows Subjected to Imposed Unsteadiness," *Journal of Fluid Mechanics*, Vol. 238, 1992, pp. 55–71.

[16]Kim, J., Moin, P., and Moser, R. D., "Turbulence Statistics in Fully-Developed Channel Flow at Low Reynolds Number," *Journal of Fluid Mechanics*, Vol. 177, 1987, pp. 133–166.

[17]Spalart, P. R., "Direct Simulation of a Turbulent Boundary Layer up to $Re_\theta = 1410$," *Journal of Fluid Mechanics*, Vol. 187, 1988, pp. 61–98.

[18]Robinson, S. K., "The Kinematics of Turbulent Boundary Layer Structure," NASA TM-103859, 1991.

[19]Spalart, P. R., and Baldwin, B. S., "Direct Simulation of a Turbulent Oscillating Boundary Layer," *Turbulent Shear Flows 6*, Springer-Verlag, New York, 1987.

[20]Hsu, C.-T., Lu, X., and Kwan, M.-K., "LES and RANS Studies of Oscillating Flows over Flat Plate," *American Society of Chemical Engineering Journal of Engineering Mechanics*, Vol. 126, No. 2, 2000, pp. 186–193.

[21] Scotti, A., and Piomelli, U., "Numerical Simulation of Pulsating Turbulent Channel Flow," *Physics of Fluids*, Vol. 13, No. 5, 2001, pp. 1367–1384.
[22] Piomelli, U., "High Reynolds Number Calculations Using the Dynamic Subgrid-Scale Stress Model," *Physics of Fluids A*, Vol. 5, No. 6, 1993, pp. 1484–1490.
[23] Germano, M., Piomelli, U., Moin, P., and Cabot, W. H., "A Dynamic Subgrid-Scale Eddy Viscosity Model," *Physics of Fluids A*, Vol. 3, No. 7, 1991, p. 1760.
[24] Lilly, D. K., "A Proposed Modification of the Germano Subgrid-Scale Closure Method," *Physics of Fluids A*, Vol. 4, No. 3, 1992, p. 633.
[25] Piomelli, U., Scotti, A., and Balaras, E., "Large-Eddy Simulation: from Desktop to Supercomputer," *Proceedings of the VECPAR2000*, edited by J. Laginha Palma and J. Dongarra, Springer-Verlag, Heidelberg, Germany, 2001, pp. 551–577.
[26] Spalart, P. R., and Allmaras, S. R., "A One-Equation Turbulence Model for Aerodynamic Flows," *La Recherche Aérospatiale*, Vol. 1, No. 1, 1994, pp. 5–21.
[27] Lam, C. K. G., and Bremhorst, K. A., "Modified Form of the k–ε Model for Predicting Wall Turbulence," *Journal of Fluids Engineering*, Vol. 103, No. 3, 1981, pp. 456–460.
[28] Patel, V. C., Rodi, W., and Scheuerer, G., "Turbulence Models for Near-Wall and Low Reynolds Number Flows: A Review," *AIAA Journal*, Vol. 23, No. 9, 1985, pp. 1308–1319.
[29] Saffman, P. G., "A Model for Inhomogeneous Turbulent Flows," *Proceedings of the Royal Society of London A*, Vol. 317, 1970, p. 417.
[30] Saffman, P. G., and Wilcox, D. C., "Turbulence Model Predictions for Turbulent Boundary Layers," *AIAA Journal*, Vol. 12, 1974, p. 541.
[31] Durbin, P. A., "Separated Flow Computations with the k–ε–v^2 Model," *AIAA Journal*, Vol. 33, No. 4, 1995, pp. 659–664.
[32] Moser, R. D., Kim, J., and Mansour, N. M., "Direct Numerical Simulation of Turbulent Channel Flow up to $Re_\tau = 590$," *Physics of Fluids*, Vol. 11, No. 4, 1999, pp. 943–945.
[33] Spalart, P. R., Jou, W. H., Strelets, M., and Allmaras, S. R., "Comments on the Feasibility of LES for Wings, and on a Hybrid RANS/LES Approach," *Advances in DNS/LES*, edited by C. Liu and Z. Liu, Greyden Press, Columbus, OH, 1997, pp. 137–148.
[34] Wilcox, D. C., "Comparison of Two-Equation Turbulence Models for Boundary Layers with Pressure Gradient," *AIAA Journal*, Vol. 31, No. 8, 1993, p. 1414.
[35] Jacobs, S. J., "Mass Transport in a Turbulent Boundary Layer Under a Progressive Water Wave," *Journal of Fluid Mechanics*, Vol. 146, 1984, p. 303.
[36] Blondeaux, P., "Turbulent Boundary Layer at the Bottom of Gravity Waves," *Journal of Hydraulics Research*, Vol. 25, No. 4, 1987, p. 447.
[37] Hsu, C.-T., Lu, X., and Kwan, M.-K., "LES and RANS Studies of Oscillating Flows over Flat Plate," *Journal of Engineering Mechanics*, Vol. 126, No. 2, 2000, p. 186.
[38] Ronneberger, D., and Ahrens, C. D., "Wall Shear Stress Caused by Signal Amplitude Perturbations of Turbulent Boundary Layer Flow: An Experimental Investigation," *Journal of Fluid Mechanics*, Vol. 83, 1977, p. 433.

R. M. C. So
Associate Editor